All-spinel oxide Josephson junctions for high-efficiency spin filtering

OPEN ACCESS
IOP Publishing
Journal of Physics: Condensed Matter
J. Phys.: Condens. Matter **30** (2018) 015804 (7pp)
https://doi.org/10.1088/1361-648X/aa9a9d

All-spinel oxide Josephson junctions for high-efficiency spin filtering

S Mesoraca[1,4], S Knudde[2], D C Leitao[2,3], S Cardoso[2,3] and M G Blamire[1]

[1] Department of Materials Science and Metallurgy, University of Cambridge, 27 Charles Babbage Road, Cambridge CB3 0FS, United Kingdom
[2] INESC-MN, Microsystems and Nanotechnologies and IN, Rua Alves Redol 9, 1000-029 Lisbon, Portugal
[3] Department of Physics, Instituto Superior Técnico, Universidade de Lisboa, 1049-001 Lisbon, Portugal

E-mail: sm2044@cam.ac.uk

Received 22 October 2017, revised 9 November 2017
Accepted for publication 14 November 2017
Published 30 November 2017

Abstract

Obtaining high efficiency spin filtering at room temperature using spinel ferromagnetic tunnel barriers has been hampered by the formation of antiphase boundaries due to their difference in lattice parameters between barrier and electrodes. In this work we demonstrate the use of $LiTi_2O_4$ thin films as electrodes in an all-spinel oxide $CoFe_2O_4$-based spin filter devices. These structures show nearly perfect epitaxy maintained throughout the structure and so minimise the potential for APBs formation. The $LiTi_2O_4$ in these devices is superconducting and so measurements at low temperature have been used to explore details of the tunnelling and Josephson junction behaviour.

Keywords: spintronics, oxides, thin films, superconductivity, pulsed laser deposition

(Some figures may appear in colour only in the online journal)

Introduction

The broad spectrum of electronic and optical properties exhibited by functional oxides offers many opportunities for microelectronic devices. In particular, the experimental growth of epitaxial oxide heterostructures has increased the development of promising novel functionalities and device concepts [1]. However, the integration of complex oxides into multilayer structures is often challenging. Lattice mismatch, structural differences and different optimum growth conditions between the oxide layers hamper the epitaxial growth of heterostructures. Of particular relevance to this paper, ultrathin films of ferromagnetic insulators (FIs) oxides can form tunnel barriers that generate nearly 100% spin-polarised currents by selectively filtering electrons according to their spins [2]. This spin-filtering process is in contrast to the classic magnetic tunnel junctions in which a non-magnetic tunnel barrier is sandwiched between two ferromagnetic electrodes [3].

The majority of FIs have Curie temperatures (T_{Curie}) well below room temperature and so, although high efficiency (~100%) spin-filtering has already been reported in a range of materials including Eu-chalcogenides [4–6], perovskites [7–10] and GdN [11, 12], potential applications are limited by the low temperatures required. In the last few years, interest has focused on spinel ferrites FIs (e.g. $NiFe_2O_4$, $CoFe_2O_4$, $MnFe_2O_4$) due to their T_{Curie} being well above room temperature [13–15]. Spin polarization of ~4–8% at room temperature has been recently reported in spinel ferrite $CoFe_2O_4$-based tunnel junctions [16, 17].

The likely reason for such low values is the formation of antiphase boundaries (APBs) in the spinel thin film barrier [18, 19], which are detrimental to spin-filter efficiency as they dramatically affect magnetic behaviour and barrier height [20, 21]. Such defects are formed due to spinels having a lattice parameter ($a = 0.83$–0.85 nm) [22], almost double that of the metallic layers (Au, Pt, $LaNiO_3$, $La_{2/3}Sr_{1/3}MnO_3$) and substrates conventionally used in spin-filter devices. Achieving high spin-filter efficiencies at room temperature may therefore

[4] Author to whom any correspondence should be addressed.

be dependent on overcoming structural and chemical defects in ultra-thin (<5 nm) epitaxial spinel ferrites films to be used in complex oxide heterostructures.

APBs can be reduced by using a spinel structure substrate ($MgAl_2O_4$) and $LiTi_2O_4$ as non-magnetic electrodes for a spin filter tunnel junction [23]. One of the few conducting spinels, $LiTi_2O_4$ is a metallic and superconducting [24] spinel (critical temperature $T_C \sim 13$ K) with a lattice parameter ($a = 0.8405$ nm) closely-lattice matched to those of the spinel $CoFe_2O_4$ ferrite and of the spinel $MgAl_2O_4$ ($a = 0.8080$ nm) substrate. The lattice mismatch to the latter is -3.8% while to $CoFe_2O_4$ ($a = 0.8392$ nm) [22] is only +0.2%.

The growth of high quality single crystal oxide thin films by pulsed laser deposition (PLD) depends on the oxygen partial pressure P_{O_2} in the chamber [23, 25–27]. $LiTi_2O_4$ has a spinel structure with equal numbers of trivalent and quadrivalent Ti cations and for P_{O_2} higher than 1×10^{-5} Torr, Ti^{3+} ions readily oxidise to Ti^{4+}, leading to the formation of $Li_4Ti_5O_{12}$, a transparent insulator phase [26]. Conversely, oxygen deficiencies are deleterious to the magnetic properties of spinel ferrite thin films [28] because the oxygen ions mediate the superexchange interaction between the magnetic ions in the spinel structure, producing the net magnetic moment in the ferrites. Thus any oxygen deficiency due to a growth at low P_{O_2}, reduces the exchange interaction between the magnetic ions, and hence, the saturation magnetization of the $CoFe_2O_4$ films. As a consequence, integrating $LiTi_2O_4$ into spinel ferrite-based spin filter junctions requires a fine tuning of the growth conditions of these two materials, requiring very different oxygen partial pressures.

In this paper we demonstrate the successful growth of $CoFe_2O_4/LiTi_2O_4$ bilayers in which $LiTi_2O_4$ maintains its metallic and superconducting properties and $CoFe_2O_4$ its insulating ferromagnetic characteristics. $LiTi_2O_4/CoFe_2O_4/LiTi_2O_4$ trilayers were processed into all-spinel oxide symmetric superconductor-insulator-superconductor (SIS) tunnel junctions. The measured current–voltage characteristics show conclusive evidence of the tunnel nature of these junctions, proving that $LiTi_2O_4$ can be used as bottom electrode in an almost APBs free tunnel junction.

Methods

$LiTi_2O_4$ and $CoFe_2O_4$ thin-films were grown by pulsed laser ablation of polycrystalline ceramic targets prepared from a mixture of Li_2CO_3 (Alfa-Aesar) and TiO_2 (Alfa-Aesar), for $Li_4Ti_5O_{12}$ [29], and from cobalt iron oxide nanopowders (Sigma-Aldrich), for $CoFe_2O_4$. The higher Li/Ti ratio (0.8) of the $Li_4Ti_5O_{12}$ target was designed to compensate for the high loss of Li during the ablation process [30]. The PLD system (KrF excimer, $\lambda = 248$ nm) was operated at an energy density of 0.7 J cm^{-2} and at a repetition rate of 5 Hz for $LiTi_2O_4$, and 2.5 J cm^{-2} and 1 Hz and for $CoFe_2O_4$.

Structural analysis was done using x-ray diffraction (XRD, PANalytical high resolution x-ray diffractometer) with monochromatised Cu$K\alpha_1$ radiation (0.154 nm). The deposition rate was determined by measuring the thickness of ultra-thin films by x-ray reflectivity analysis, allowing the controlled deposition of thicker films. The films' transport measurements were performed by four-wire method between 300 K and 4.2 K by direct Al-bonding to unpatterned films. Magnetic properties of the films were measured using a vibrating sample magnetometer (VSM) with a maximum dc magnetic field of 1 T.

The SIS trilayers were patterned into square pillars (size ranging from 2×2 μm^2 to 4×4 μm^2) by optical laser lithography, ion-milling and lift-off steps. The ion milling procedure was performed using a self-aligned process for junction fabrication [31] in a Nordiko 3600 ion beam deposition system [32] with an Ar^+ beam (current density ~340 μA cm^{-2}), first at an angle with respect to the substrate of 70° down to the $CoFe_2O_4$ barrier and subsequently at 40° until it penetrated the bottom $LiTi_2O_4$ electrode. This ensured a barrier with steep profile and well controlled nominal size, while avoiding material re-deposition on the sidewalls [33, 34]. A 100 nm-thick Al_2O_3 layer was deposited by RF sputtering for passivation and lateral insulation of the pillars. The top electrode (Au(100 nm)/Cr(10 nm)) was deposited in an Alcatel SCM450 multi-target DC magnetron sputtering system. Before the patterning process, the structure was covered with a 15 nm-thick Ta anti-reflection layer, deposited by ion beam deposition in a Nordiko 3000 system [35], to reduce specular reflections of the laser during the lithography process.

Device transport properties were measured with a four-probe dc current-biased method in a closed-cycle helium cryostat. A differential conductance spectrum was obtained by numerically differentiating the *I–V* characteristic after applying a moving average window to smooth the data.

Results and discussion

Bilayer characterisation

PLD-growth of $LiTi_2O_4$ requires reducting conditions, and thus during film growth, the deposition chamber was evacuated to 1×10^{-6} Torr and the substrate temperature was kept at 800 °C; this is the optimal temperature to reduce Li segregation at the surface [23]. During the subsequent growth of $CoFe_2O_4$, the temperature of the substrate was lowered to 450 °C to avoid any unfavourable oxidation of the deposited $LiTi_2O_4$ layer. Thereafter high purity oxygen was injected into the chamber and the P_{O_2} was maintained at 2.5×10^{-4} Torr, to limit the formation of oxygen deficiencies in the magnetic layer. In this way, the chemical potential of oxygen ions was lower and the oxidation of Ti^{3+} into Ti^{4+} could be avoided, keeping $LiTi_2O_4$ in its metallic, superconducting phase. To verify epitaxy and bulk phase purity of the deposited films, we measured out-of-plane XRD patterns for a $CoFe_2O_4$(60 nm)/$LiTi_2O_4$(200 nm) bilayer.

The XRD pattern (figure 1) shows clear (1 1 1) and (2 2 2) Bragg reflection peaks of the films and those of the underlying $MgAl_2O_4$(1 1 1) substrate. No undesired phase or orientation of either $LiTi_2O_4$ or $CoFe_2O_4$ is observed in the pattern, demonstrating that both layers are in single phase and highly oriented. The overlap of the reflection peaks of the two films forming the bilayer, due to their close lattice match, is clear in the inset of figure 1 where the (2 2 2) reflection peak of the bilayer is compared with the reflections of a single $LiTi_2O_4$ (200 nm) film and a single $CoFe_2O_4$(60 nm) film grown on $MgAl_2O_4$ (1 1 1).

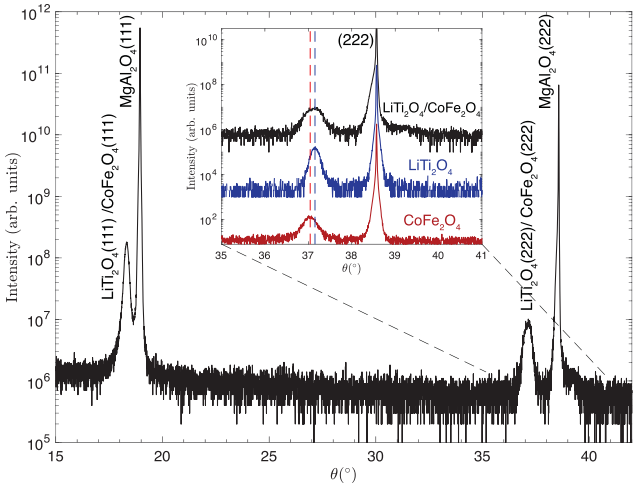

Figure 1. XRD pattern for a $CoFe_2O_4$ (60 nm)/$LiTi_2O_4$ (200 nm) bilayer around the symmetric (1 1 1) $MgAl_2O_4$ reflection. Inset compares XRD pattern of the bilayer (black) with those of a 60 nm-thick $CoFe_2O_4$ (red) and 200 nm-thick $LiTi_2O_4$ (blue) single films.

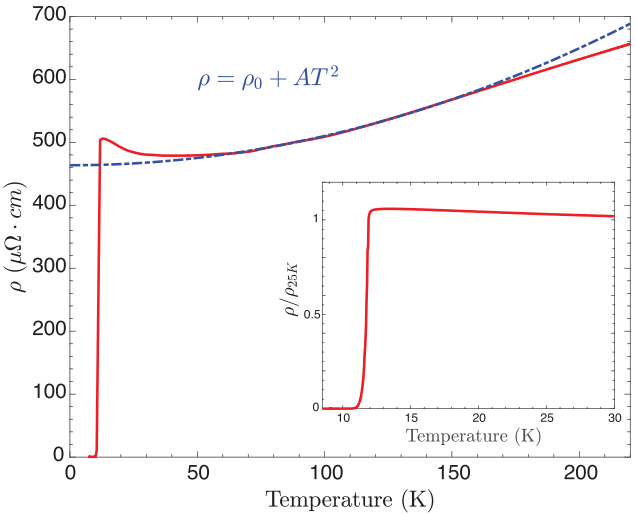

Figure 2. Temperature dependence of resistivity for a $CoFe_2O_4$ (10 nm)/$LiTi_2O_4$ (50 nm) bilayer. The blue-dotted line is the quadratic $\rho = \rho_0 + AT^2$ fit in the temperature range 50–150 K. The inset shows the superconducting transition at $T_c = 11.5$ K.

Temperature-dependent resistivity measurement of a $CoFe_2O_4$(10 nm)/$LiTi_2O_4$(50 nm) bilayer shows metallic behaviour (figure 2). Moreover, the bilayer displays a superconducting transition at $T_C = 11.5$ K, confirming that the bottom layer has kept its metallic-superconducting phase without undergoing any oxidation due to the growth of $CoFe_2O_4$. The T_C is in good agreement with previous findings on single $LiTi_2O_4$ films [23, 25, 26]. The width of the superconducting transition is less than 0.4 K (figure 2, inset). The Fermi liquid behaviour of the bilayer is confirmed by the variation of resistivity as T^2 from 50 to 150 K (blue-dashed line). The residual resistivity ρ_0 and the residual resistivity ratio RRR $= \rho_{300\,K}/\rho_{25\,K}$ of the films were 460 $\mu\Omega$ cm and 1.5, respectively, in accordance with recent publications [23, 25–27, 36]. At temperatures below 20 K the bilayer exhibits

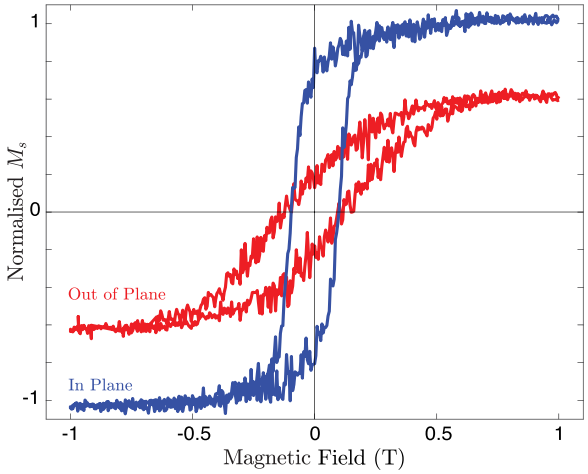

Figure 3. Normalised in-plane (blue) and out-of-plane (red) magnetic hysteresis loops at room temperature of a $CoFe_2O_4$(60 nm)/$LiTi_2O_4$(50 nm) bilayer grown on $MgAl_2O_4$ (1 1 1). The diamagnetic contribution of the substrate has been subtracted from the measured signal and the hysteresis loops are normalised to the in-plane M_s value at 1 T.

an increase in resistance, characteristic of weak localization in disordered 2D films [37].

The room temperature magnetic hysteresis loops of a $CoFe_2O_4$(60 nm)/$LiTi_2O_4$(50 nm) bilayer grown on $MgAl_2O_4$(1 1 1) substrate are shown in figure 3. The magnetic layer is ferromagnetically easy in the film plane, with a hard direction normal to the film. The in-plane magnetization (M_s) at 1 T and the coercive field were 200 emu cm^{-3} (or a magnetic moment of 1.6 μ_B per formula unit) and 95 mT, respectively. This magnetic moment value is lower than the maximum 3 μ_B, theoretically obtained for bulk $CoFe_2O_4$ with an inverse spinel structure [38].

The decreased M_s is consistent with previous reports [28] on $CoFe_2O_4$ films grown at low P_{O_2} and low temperature, and was expected due to the conditions required to avoid any oxidation of the underlying $LiTi_2O_4$. In a spin filter device, the tunnelling spin currents depend exponentially on the barrier height difference between the two spins. Thus, a lower than expected exchange energy of the FI, due to the lower M_s values, can still produce a high polarisation of the current.

Several other approaches were followed in order to combine $LiTi_2O_4$ and $CoFe_2O_4$ in a bilayer without detrimentally affect each other during growth: (i) a few capping monolayers of $CoFe_2O_4$ were grown at the same reduced P_{O_2} environment of $LiTi_2O_4$, in order to not expose the latter to oxygen during the growth of the subsequent monolayers of $CoFe_2O_4$ in higher P_{O_2} to increase the magnetic moment of latter; (ii) the bilayer was grown entirely in reduced oxygen environment and annealed at different P_{O_2} and at different temperatures, to compensate for the oxygen deficiencies in the $CoFe_2O_4$ layer; (iii) a mixture of N_2O/O_2 instead of O_2 was used, as suggested by Hassan *et al* [39], to reduce the chemical potential of the oxygen ions. In all cases, though an increased M_s of the $CoFe_2O_4$ layer could be observed, the underlying $LiTi_2O_4$ of the bilayers showed insulating behaviour indicating an

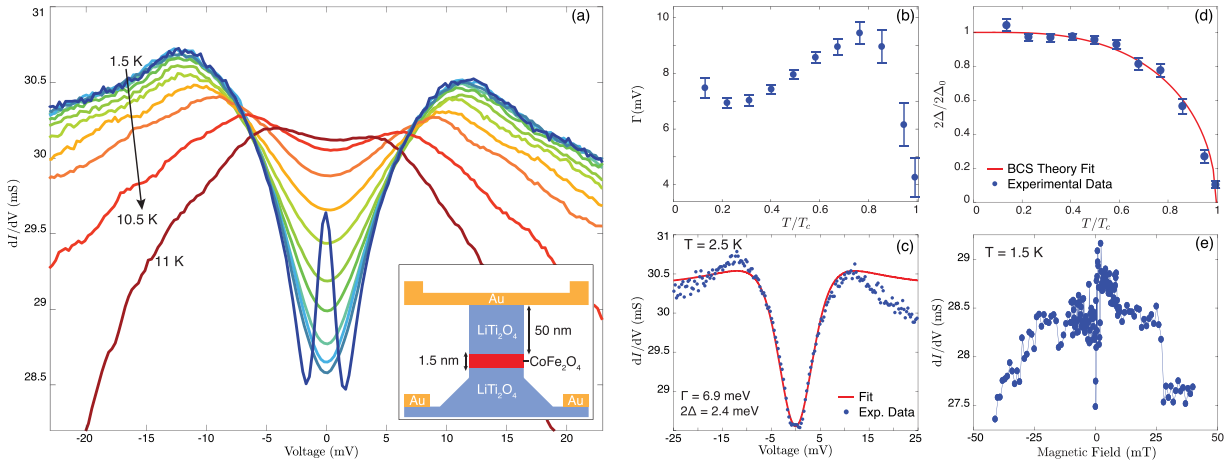

Figure 4. (a) Differential conductance dI/dV versus bias voltage from 1.5 to 10.5 K with 1 K increments and at 11 K in zero field for a $LiTi_2O_4$(50 nm)/$CoFe_2O_4$(1.5 nm)/$LiTi_2O_4$(50 nm) junction. The size of the junction is 3×3 μm^2. The inset shows the schematic cross section of the side view of the micro-tunnel junction with bottom and top contact leads. (b) Normalised temperature evolution of the Dynes fitting parameter Γ. (c) The smeared BCS s-wave model fit to the dI/dV versus bias voltage characteristic at 2.5 K with $2\Delta = 2.4$ meV and $\Gamma = 6.9$ meV. (d) Temperature dependence of normalised energy gap 2Δ and BCS fit. (e) Field dependence of the supercurrent peak appearing at 1.5 K. The error bars represent the s.e. in the fit to the dI/dV data.

oxidation of the Ti^{3+} ions and the formation of the unwanted $Li_4Ti_5O_{12}$ phase.

Tunnel junction characterisation

To prove the suitability of $LiTi_2O_4$ as an electrode in an almost defect-free all-spinel oxide spin filter junction we have grown a symmetric superconducting tunnel junction of the form $LiTi_2O_4$(50 nm)/$CoFe_2O_4$(1–3 nm)/$LiTi_2O_4$(50 nm). For this purpose, a second layer of $LiTi_2O_4$ was grown on top of the $CoFe_2O_4$(1–3 nm)/$LiTi_2O_4$(50 nm) bilayers. These oxide heterostructures were then patterned into micro-pillars as described earlier (figure 4(a), inset). The dynamic conductance of a representative sample is depicted in figure 4(a): the dI/dV spectrum exhibits a characteristic superconducting energy gap structure with a dip around the zero bias and strongly smeared coherence peaks. At temperatures approaching the T_c of $LiTi_2O_4$, the gap decreases until it disappears for higher temperatures. The decrease of the conductance observed at voltages above 2Δ is most likely due to flux flow and heating in the electrodes at high current densities ~15 kA cm^{-2}. Similar behaviours are common in tunnel junctions based on high T_C superconductors [40]. The broadening of the coherence peaks is an evidence for the smearing of the interfacial density of states due to the proximity effect of a ferromagnetic Mott insulator, which shortens the quasiparticle lifetime [41–43]. Another contributing factor to the smearing of the dI/dV curves could be the possible stoichiometric inhomogeneity between two $LiTi_2O_4$ electrodes as a consequence of their different growth conditions.

The form of the dI/dV spectra implies that at least one of the $LiTi_2O_4$ electrodes preserves a superconducting density of states at the $CoFe_2O_4$ interface. We will begin by assuming that both electrodes are superconducting and then justify this in the light of the available information.

A simplified BCS smeared superconductor-insulator-normal metal (SIN) model was employed to fit the dI/dV raw data and estimate the energy gap Δ. According to this model $\frac{dI}{dV} \propto \mathrm{Re}\left[\frac{(|E-eV|-i\Gamma)}{\left((E-eV)^2-\Delta^2\right)^{1/2}}\right]$, in the limit of low bias voltages and for low temperatures [42]. Here Γ is the Dynes parameter accounting for the experimentally observed broadening [41] and for large values of Γ in both electrodes this model can also model SIS quasiparticle conductance spectra if Δ is replaced by 2Δ. The fitting values of Γ are shown in figure 4(b). In figure 4(c) it is shown the fit to a dI/dV curve collected at 2.5 K with $2\Delta = 2.47$ meV and $\Gamma = 6.9$ meV. The peak height and the gap structure of the raw data are quite accurately reproduced by the fit. The superconducting energy gap width $2\Delta(T)$ was determined from this data. The dependence of 2Δ on the temperature (shown in figure 4(d)) fits well with BCS-type temperature dependence [44], $2\Delta(T) = 2\Delta_0 \tanh(1.74\sqrt{(T_c - T)/T}$ (solid line)) confirming a superconducting behaviour. The fitting parameters are $2\Delta_0 = (2.6 \pm 0.1)$ meV, which is lower than the one reported in previous findings [27, 45, 46], and $T_C = (11.0 \pm 0.3)$ K, in accordance with the value measured in our bilayers. Consequently, we find a $2\Delta_0/k_bT_c$ ratio of 2.8 ± 0.2, which is less than the typical values ranging between 3 and 4.5 for BCS like superconductors but in agreement with recent scanning tunnelling spectroscopy on $LiTi_2O_4$ films [47] suggesting a modified superconductivity on the surface due to a non-stoichiometric surface layer. Another contributing factor to the reduced gap value is the suppression of the order parameter in the $LiTi_2O_4$ electrodes due to the proximity with the $CoFe_2O_4$ magnetic barrier; this is also presumably responsible for the large value of Γ. If we assumed SIN behaviour, our estimate for 2Δ would be doubled to 5 meV that is significantly larger than reported previously and so appears unreasonable.

SIS junctions would normally be expected to show a Josephson supercurrent with a maximum value of $\pi\Delta/2R_j$ where R_j is the junction normal state resistance, but for strongly spin filtering barriers, this is expected to be substantially reduced because the tunnelling of conventional

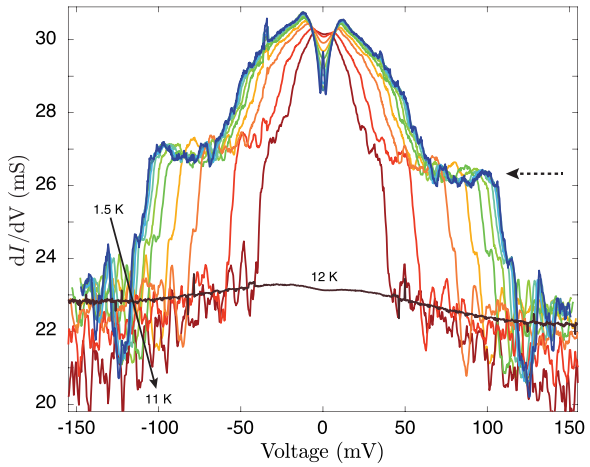

Figure 5. Differential conductance d*I*/d*V* versus bias voltage from 1.5 to 10.5 K with 1 K increments and at 11 K and 12 K in zero field for a $LiTi_2O_4$(50 nm)/$CoFe_2O_4$(1.5 nm)/$LiTi_2O_4$(50 nm) junction collected at higher bias voltages.

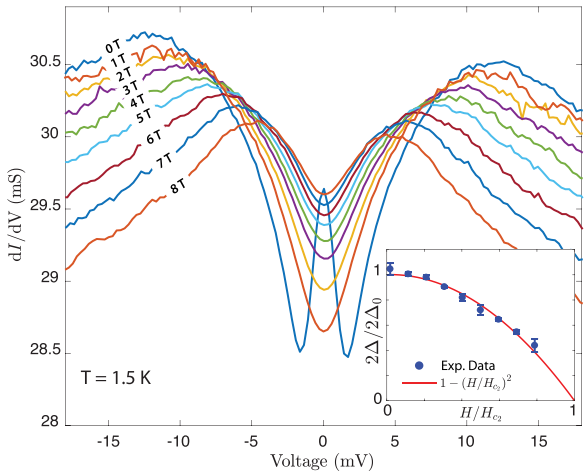

Figure 6. Differential conductance d*I*/d*V* versus bias voltage at 1.5 K from 0 T to 8 T with 1 T increments for a $LiTi_2O_4$(50 nm)/$CoFe_2O_4$(1.5 nm)/$LiTi_2O_4$(50 nm) junction. Inset, normalised energy gap $2\Delta/2\Delta_0$, at 1.5 K, decreasing as $1 - [H/H_{c2}(T)]^2$. The error bars represent the s.e. in the fit to the dI/dV data.

singlet Cooper pairs is blocked [48]. At the lowest temperatures a zero bias peak appears in low-resistance junctions ($R_j \sim 0.05$ kΩ) while in medium-resistance junctions ($R_j \sim 0.9$ kΩ) this feature is not observed—as might be expected given the experimental noise. Although this feature might be related to the flow of a Josephson supercurrent in the junction, its disappearance at temperatures well below T_c is inconsistent with standard behaviour. Similarly, the dependence of the supercurrent peak on an in-plane external applied field (shown in figure 4(e)) does not show the Fraunhofer-like periodic suppression of the peak characteristic of Josephson tunnel junctions. Indeed, the appearance of the zero-bias peak may also be related to the presence of Andreev bound states [49].

The d*I*/d*V* curves collected at higher biases (figure 5) reveal an interesting midpoint state between the low bias SIS-state (i.e. both electrodes are superconducting) and the state in which the electrodes are metallic (normal state) at high bias. This conductance midpoint state is related to bias voltages at which one of the $LiTi_2O_4$ electrodes is superconducting while the other is metallic. The midpoint state, identified by the dashed arrow in figure 5, indicates that the electrodes are in different superconducting states. For high biases the two electrodes are in their normal state and the conductance of the junction is equal to that measured at temperatures above T_C (12 K). At higher temperatures, lower biases are needed to turn the electrodes from the superconducting state to the metallic-normal state. This confirms the SIS-nature of the junctions, while the presence of two distinct conductance-states is another validation of a stoichiometric inhomogeneity between two superconducting $LiTi_2O_4$ electrodes.

d*I*/d*V* spectra collected at 1.5 K at different out of plane applied magnetic fields are shown in figure 6. The closing of the peak position along with the closing of the gap and the suppression of the superconducting peak for values approaching the $LiTi_2O_4$ upper critical field H_{c2}, are clearly visible. The scaling law follows a field quadratic-dependence $\Delta(B,T) \sim \Delta_0 - [H/H_{c2}(T)]^2$, as recently reported in point contact spectra [27]. The fit, shown in the inset of figure 6, gives an extracted value of H_{c2} at 2 K of ~10.8 T, which is consistent with previous results [45, 46].

Figure 7 shows the temperature dependence of a typical $LiTi_2O_4$/$CoFe_2O_4$/$LiTi_2O_4$ junction resistance with 1.5 nm $CoFe_2O_4$ barrier measured by applying a 0.1 mA current. A sharp drop in resistance is seen at the $LiTi_2O_4$ superconducting transition due to the disappearance of the in-series resistance of the leads. At higher temperatures the resistance is not exponentially increasing with decreasing temperature, which is the behaviour for a semiconducting non-magnetic barrier [50], but is instead continuously dropping with temperature. The temperature dependence of the resistance of the $LiTi_2O_4$ bottom lead of the same junction was measured (inset (b), figure 7) to verify that the decreasing behaviour of R_j is attributable to tunnelling current flowing across the tunnel junction and not across any series resistances, which would explain the decreasing behaviour. This is confirmed by difference in the order of magnitude between the resistance of junction ~10^1 Ω and the resistance of the bottom-lead ~10^2 Ω. In addition, large contributions of non-tunnelling (leakage) conductance to the dominant tunnel conductance due to shorts between the two electrodes can be also ruled out since R_j is non-zero for temperature below T_C, as opposed to the two $LiTi_2O_4$ superconducting electrodes which show zero resistance.

Moreover, the resistance increases with decreasing temperature below T_C, due to the fact that there are no available states for tunnelling at the Fermi energy level for measurements voltages much less than Δ. In this case the conductance is dominated by thermal excitation of quasi-particles across the gap and, as temperature decreases, the number of thermally excited quasi-particle states decreases exponentially, resulting in an increases of the sub-gap resistance for decreasing temperature. These behaviours confirm that the mechanism of charge transport in the junctions is predominantly tunnelling in nature and thus, the drop in R_j with decreasing temperature observed across the entire temperature range above T_C may

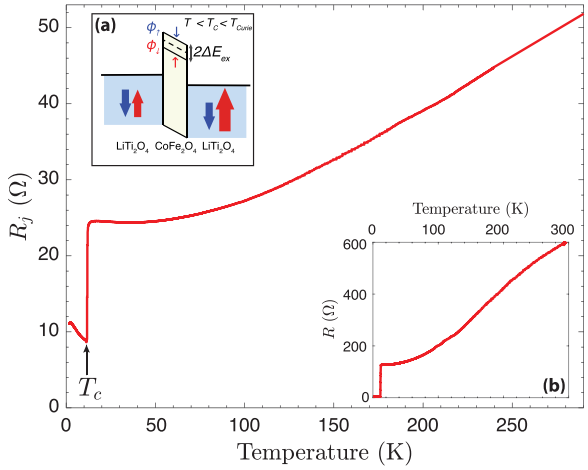

Figure 7. Junction resistance versus temperature dependence of a $LiTi_2O_4$(50 nm)/$CoFe_2O_4$(1.5 nm)/$LiTi_2O_4$(50 nm) junction measured at a constant dc bias of 0.1 mA in a two-wire configuration. Inset (a), band diagram for a spin filter device. Inset (b), resistance versus temperature of the bottom $LiTi_2O_4$-lead of the same junction and measured in the same two-wire configuration.

be a consequence of the exchange splitting of the magnetic tunnel barrier, leading to a temperature dependent reduction of the barrier height of one spin (inset (a), figure 7). The T_{Curie} of $CoFe_2O_4$ is well above room temperature, so the absence of the typical change from semiconducting behaviour to metallic-like behaviour at T_{Curie}, due to onset of spin filtering, reported in spin filtering devices of this type [8, 12] is expected in our range of measurement.

Conclusions

In summary, we demonstrated the successful superconducting tunnel process in an all-spinel SIS tunnel junctions with $CoFe_2O_4$ as FI barrier and $LiTi_2O_4$ as electrodes grown on $MgAl_2O_4$ substrates. The integration of the metallic-superconducting $LiTi_2O_4$ in tunnel junctions offers new possibilities in the quest of achieving high efficiency room temperature spin filtering due to lattice match with the spinel Co-ferrite, reducing APBs.

The $CoFe_2O_4$/$LiTi_2O_4$ holds the potential for all-oxide magnetic tunnel junctions with efficient spin filtering properties at room temperature. An estimation of the polarisation of the current could not be performed by extrapolating the temperature dependence of R_j from the high temperature ($> T_{\text{Curie}}$) regime as T_{Curie} in this case is well above room temperature. This capability could be investigated by tunnel magnetoresistance-like experiments by replacing the top $LiTi_2O_4$ electrode with a spinel ferromagnet (Fe_3O_4) decoupled from the $CoFe_2O_4$ by a thin insulating layer of $MgAl_2O_4$, as suggested by promising tunnelling spectroscopy study on junctions with Au electrode [13]. The perfect epitaxy and lattice match between all the layers of such Fe_3O_4/$MgAl_2O_4$/$CoFe_2O_4$/$LiTi_2O_4$ devices grown on $MgAl_2O_4$ substrates, paves the way to high efficiency spin filtering at room temperature.

Acknowledgments

The research leading to these results has received funding from the European Union Seventh Framework Programme ([FP7/2007-2013] [FP7/2007-2011]) under grant agreement 316657 (SpinIcur).

D C Leitao acknowledges financial support through FSE/POPH. INESC-MN acknowledges FCT funding through the IN Associated Laboratory.

ORCID iDs

S Mesoraca https://orcid.org/0000-0001-5745-5426
D C Leitao https://orcid.org/0000-0001-8419-2967

References

[1] Bibes M, Villegas J E and Barthélémy A 2011 *Adv. Phys.* **60** 5
[2] Moodera J S, Santos T S and Nagahama T 2007 *J. Phys.: Condens. Matter* **19** 165202
[3] Moodera J S, Kinder L R, Wong T M and Meservey R 1995 *Phys. Rev. Lett.* **74** 3273
[4] Moodera J, Hao X, Gibson G and Meservey R 1988 *Phys. Rev. Lett.* **61** 637
[5] Moodera J S, Meservey R and Hao X 1993 *Phys. Rev. Lett.* **70** 853
[6] Santos T and Moodera J 2004 *Phys. Rev.* B **69** 241203
[7] Gajek M, Bibes M, Barthélémy A, Bouzehouane K, Fusil S, Varela M, Fontcuberta J and Fert A 2005 *Phys. Rev.* B **72** 20406
[8] Prasad B, Egilmez M, Schoofs F, Fix T, Vickers M E, Zhang W, Jian J, Wang H and Blamire M G 2014 *Nano Lett.* **14** 2789
[9] Prasad B, Zhang W, Jian J, Wang H and Blamire M G 2015 *Adv. Mater.* **27** 3079
[10] Harada T, Ohkubo I, Lippmaa M, Sakurai Y, Matsumoto Y, Muto S, Koinuma H and Oshima M 2012 *Phys. Rev. Lett.* **109** 76602
[11] Pal A, Senapati K, Barber Z H and Blamire M G 2013 *Adv. Mater.* **25** 5581
[12] Senapati K, Blamire M G and Barber Z H 2011 *Nat. Mater.* **10** 849
[13] Chapline M and Wang S 2006 *Phys. Rev.* B **74** 14418
[14] Lüders U, Barthélémy A, Bibes M, Bouzehouane K, Fusil S, Jacquet E, Contour J-P, Bobo J-F, Fontcuberta J and Fert A 2006 *Adv. Mater.* **18** 1733
[15] Matzen S, Moussy J-B, Miao G X and Moodera J S 2013 *Phys. Rev.* B **87** 184422
[16] Ramos A V, Guittet M-J, Moussy J-B, Mattana R, Deranlot C, Petroff F and Gatel C 2007 *Appl. Phys. Lett.* **91** 122107
[17] Matzen S, Moussy J-B, Mattana R, Bouzehouane K, Deranlot C and Petroff F 2012 *Appl. Phys. Lett.* **101** 42409
[18] Datta R, Loukya B, Li N and Gupta A 2012 *J. Cryst. Growth* **345** 44
[19] Ma J X, Mazumdar D, Kim G, Sato H, Bao N Z and Gupta A 2010 *J. Appl. Phys.* **108** 63917
[20] Margulies D, Parker F and Rudee M 1997 *Phys. Rev. Lett.* **953** 2
[21] Moussy J-B *et al* 2004 *Phys. Rev.* B **70** 174448
[22] Moussy J-B 2013 *J. Phys. D: Appl. Phys.* **46** 143001
[23] Mesoraca S, Kleibeuker J E, Prasad B, MacManus-Driscoll J L and Blamire M G 2016 *J. Cryst. Growth* **454** 134

[24] Johnston D, Prakash H, Zachariasen W H and Viswanathan R 1973 *Mater. Res. Bull.* **8** 777
[25] Chopdekar R V, Wong F J, Takamura Y, Arenholz E and Suzuki Y 2009 *Physica* C **469** 1885
[26] Kumatani A, Ohsawa T, Shimizu R, Takagi Y, Shiraki S and Hitosugi T 2012 *Appl. Phys. Lett.* **101** 123103
[27] Jin K *et al* 2015 *Nat. Commun.* **6** 7183
[28] Zhou J, He H and Nan C-W 2007 *Appl. Surf. Sci.* **253** 7456
[29] Hirayama M, Kim K, Toujigamori T, Cho W and Kanno R 2011 *Dalton Trans.* **40** 2882
[30] Dumont T, Lippert T, Döbeli M, Grimmer H, Ufheil J, Novák P, Würsig A, Vogt U and Wokaun A 2006 *Appl. Surf. Sci.* **252** 4902
[31] Gallagher W J *et al* 1997 *J. Appl. Phys.* **81** 3741
[32] Cardoso S, Macedo R J, Ferreira R, Augusto A, Wisniowski P and Freitas P P 2008 *J. Appl. Phys.* **103** 07A905
[33] Leitao D C, Silva A V, Ferreira R, Paz E, Deepack F L and Cardoso S 2014 *J. Appl. Phys.* **526** 17E526
[34] Jeong J and Endoh T 2017 *Japan. J. Appl. Phys.* **56** 04CE09
[35] Gehanno V, Freitas P P, Veloso A, Ferrira J, Almeida B, Soasa J B, Kling A, Soares J C and da Silva M F 1999 *IEEE Trans. Magn.* **35** 4361
[36] Oshima T, Yokoyama K, Niwa M and Ohtomo A 2015 *J. Cryst. Growth* **419** 153
[37] Li T and Sheng P 1996 *Phys. Rev.* B **53** R13268
[38] Szotek Z, Temmerman W, Ködderitzsch D, Svane A, Petit L and Winter H 2006 *Phys. Rev.* B **74** 174431
[39] Hassan R S, Viart N, Ulhaq-Bouillet C, Loison J L, Versini G, Vola J P, Crégut O, Pourroy G, Muller D and Chateigner D 2007 *Thin Solid Films* **515** 2943
[40] Cybart S A, Cho E Y, Wong T J, Wehlin B H, Ma M K, Huynh C and Dynes R C 2015 *Nat. Nanotechnol.* **10** 598
[41] Dynes R C C, Na V, Narayanamurti V and Garno J P 1978 *Phys. Rev. Lett.* **41** 1509
[42] Ozyuzer L, Zasadzinski J F, Kendziora C and Gray K E 2000 *Phys. Rev.* B **61** 3629
[43] Pal A and Blamire M G 2015 *Phys. Rev.* B **92** 180510
[44] Bardeen J, Cooper L and Schrieffer J 1957 *Phys. Rev.* **108** 1175
[45] Tang L, Zou P Y, Shan L, Dong A F, Che G C and Wen H H 2006 *Phys. Rev.* B **73** 184521
[46] Sun C P, Lin J-Y, Mollah S, Ho P L, Yang H D, Hsu F C, Liao Y C and Wu M K 2004 *Phys. Rev.* B **70** 54519
[47] Okada Y, Ando Y, Shimizu R, Minamitani E, Shiraki S, Watanabe S and Hitosugi T 2017 *Nat. Commun.* **8** 15975
[48] Bergeret F S, Verso A and Volkov A F 2012 *Phys. Rev.* B **86** 60506
[49] Greene L H *et al* 2003 *Phys. C Supercond.* **387** 162
[50] Moodera J S and Mathon G 1999 *J. Magn. Magn. Mater.* **200** 248